

Representing Structural Isomer Effects in a Coarse-Grained Model of Thermoplastic Polymer Poly(etherketoneketone)

Chris Jones,[†] Jenny Fothergill,[†] Rainier Barrett,[†] Lina N. Ghanbari,[‡] Nicholas R Enos,[‡] Olivia McNair,[‡] Jeffrey Wiggins,[‡] and Eric Jankowski^{*,†}

†Micron School of Materials Science and Engineering, Boise State University

‡School of Polymer Science and Engineering, University of Southern Mississippi

E-mail: ericjankowski@boisestate.edu

Introduction

Thermoplastic composites are promising next-generation aerospace materials due to their low weight, high strengths, and the ability to thermally weld parts for uniform, fastener-free joints.^{1–5} These composites can be made from carbon fiber weaves or unidirectional tapes that are impregnated with a thermoplastic polymer-based matrix material that softens when heated. Panels and parts are made from layering composites into forms that undergo high-temperature consolidation. The resulting parts can be welded together by locally heating contacting surfaces at the interface between two parts.

Welding together small parts into larger structures presents both opportunities and challenges. Opportunity lies in the ability to mass produce the small parts, which can be individually checked for quality control. The challenge lies in ensuring the strength and failure behavior of the large structures, particularly at the welds, because no stress-bearing carbon

fibers span these joints.^{6,7}

The strength of welds therefore depends on the entanglements of the polymer molecules that interpenetrate across the interface.⁸ Understanding and improving thermoplastic composite welds, therefore, depends on mechanistic understanding of how the matrix chemistry, polydispersity, defects, and surface preparation all influence the polymer structure that results from welding at a particular temperature and pressure. With so many processing parameters to tune, identifying the optimal combination is an intractably large design problem to tackle by trial and error.

Molecular dynamics (MD) simulations are a promising tool for providing both mechanistic insight into thermoplastic welding, and for serving as a surrogate to trial-and-error experiments. However, because the timescales of polymer dynamics are long (e.g., many minutes for some polymer crystallization^{9–11}), and because the length scales of structural periodicities can exceed many nanometers, MD simulations of atomic polymer representations are prohibitively expensive.^{12–14} Computational costs for structurally complex, slow-relaxing systems compound because the time it takes to evaluate one time step forward in MD at best scales $O(N \log N)$ with the number of simulation elements (atoms) N , and $N \approx 5e4 – 1e6$ atoms are usually needed to represent these polymers, and the more atoms the higher the number of time steps it takes for the system to relax to equilibrium. Consequently, a doubling of the length scales observed in a simulation requires 8x more simulation elements, which would in the best case require 8x more time steps to relax, and 16.6x more seconds per step, or a simulation that takes 133 times as long to run.

Even worse are the time dynamics that matter for welding. In order for a strong weld to form, inter-penetration of polymer chains (entanglement) needs to occur across the interface of two pieces of the material,^{15,16} as opposed to chemical bond formation, such as in epoxy and thermoset materials.^{17,18} In order to accurately model polymer entanglements, and the role they play in thermoplastic welding and mechanical strength, two aspects that need to be considered are the entanglement length (N_e) and the chain diffusion behavior in the presence

of entanglements, both of which are described by the reptation model of Edwards and De Gennes.^{19,20} Therefore, thermoplastic weld models need to include chain lengths long enough to result in the formation of entanglements and access reptation timescales. To this end, we employ a coarse-grained (CG) approach needed in order to achieve time and length scales that are relevant for the thermal welding process of polymers.

There are multiple approaches for creating coarse-grained potentials, each with their own advantages and disadvantages, and each geared toward optimizing different aspects of the underlying physics and material properties. Several reviews discussing these coarse-graining methods exist; in particular, we direct the reader towards work from Gartner and Jayaraman, 2019 and Dhamankar and Webb, 2021 which emphasize these coarse-graining approaches in the context of polymers.^{21,22} In brief, some well-known examples include force matching, relative entropy and iterative Boltzmann inversion (IBI). Force matching aims to minimize the error between the forces in the coarse-grained model and the net forces in the atomistic system projected onto the coarse-grained mapping scheme, and therefore should result in an equivalent trajectory.^{23,24} Relative entropy is an iterative method that minimizes statistical differences between the target and coarse-grained models.^{25,26} While relative entropy is a powerful approach that can reproduce both equilibrium structure and forces from a target model, implementation is non-trivial, and the iterative updates to the coarse model are not as straight forward as either force matching or structure matching methods.²² IBI is designed to generate coarse-grained potentials that match fine-grained structural distributions such as the radial distribution function (RDF) and bond, angle and dihedral probability distributions when learning intramolecular and intermolecular potentials respectively.²⁷ IBI is commonly used for coarse-graining polymer systems.^{28–32} One major drawback of using IBI is that the resulting potentials are generally not transferable across thermodynamic state points. However, it has been shown that using a weighted average across multiple state points when learning potentials via IBI can create coarse models that are transferable within the bounds of the state points used. This method, termed multi-state iterative Boltzmann inversion

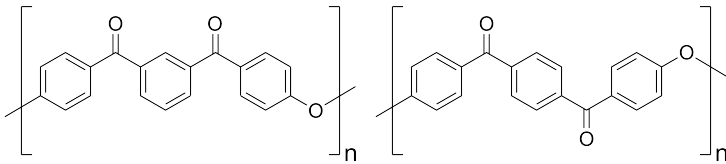


Figure 1: Two isomers of the PEKK repeat units: Meta (left, from isophthalic acid (I) and para (right, from terephthalic acid (T)) orientations of ketone groups across the central phenyl ring. The higher the T/I ratio of monomers used to synthesize the copolymer, the straighter the chains and the higher the T_m .

(MSIBI), developed by Moore et al. has been successfully applied from relatively simple systems such as Lennard Jones fluids, propane, and water to more complex systems such as lipid bilayers.^{33–37}

PEKK

Poly(ether-ketone-ketone) (PEKK) is an aerospace composite matrix material that offers high mechanical strength, chemical resistance, and thermal stability.^{12,38,39} It is a linear thermoplastic polymer in the polyaryl-ether-ketone family made from repeat units of phenyl rings with ether-ketone-ketone linkage groups as shown in Figure 1. The molecular structure and material properties of PEKK depend on the amount of para- and meta- ketone linkages (Figure 1) comprising the chain. For para linkages (Figure 1 (b)), the 180° relative orientation of ketone moieties results in straighter chain sections. Meta linkages have a 120° angle across their phenyl ring (Figure 1 (a)). The relative amount of para and meta linkages depends on the amount of terephthalic (T) and isophthalic (I) precursors used in synthesis, respectively (Figure 1), which influences crystallization kinetics, chain packing structure, and the melting temperature (T_m).¹¹ Consequently, PEKK can be thought of as a random co-polymer of para and meta isomers of ether-ketone-ketone repeat units, where the relative amount of each repeat unit is given by the T/I ratio. Thus, “T/I ratio” reports the relative *amount* of Terephthalic linkages (e.g., a system with a T/I ratio of 80/20 is one with 80 percent para linkages and 20 percent meta linkages), and avoids nomenclature clashes with, for example, temperature (kT)

Lower T/I ratios (i.e. decreasing the number of para linkages) results in lower T_m , slower crystallization kinetics, and decreased crystallinity.^{11,38,40,41} For example, PEKK(T/I=1.0) has a reported T_m of 410° C while PEKK(T/I=0.60) melts near 300° C.^{38,40} However, the T/I ratio has little effect on the glass transition temperature (T_g).⁴⁰ As a consequence of this T/I ratio effect, the thermal properties of PEKK can be tuned by choosing the best suited T/I ratio for the application. In the case of high-throughput manufacturing, lower T/I ratios might be preferred to induce faster processing times via the decrease in T_m . Additionally, PEKK materials with lower processing temperatures help to avoid the undesirable effects of melt-state degradation that have been reported in PAEK polymers.^{42–44} Alternatively, if a larger degree of crystallinity is favored, then high T/I ratios may be preferred. Regardless of the application, it is apparent that the T/I ratio of the PEKK matrix material offers another adjustable parameter in an already extensive design-space of thermoplastic composite manufacturing.//

In this paper, we present a CG model of PEKK, develop a CG forcefield using MSIBI, and introduce a strategy that encodes the T/I ratio effect within one component of the overall CG potential, making the model transferable across varying T/I ratios. The approach significantly enhances computational efficiency while delivering structural accuracy. This brings us closer to achieving the necessary time and length scales for modeling the welding of PEKK polymer interfaces.

Models

In this section, we describe the United Atom (UA) model upon which the coarse-grained (CG) model is built, and the unique modeling considerations that arise in the development of a coarse-grained model of PEKK.

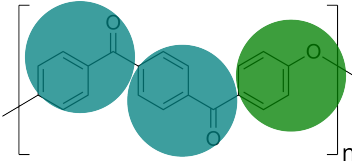


Figure 2: Coarse-grained mapping scheme with E (Green) and K (Blue) beads.

United Atom PEKK

We use a UA model to generate “target” structural distributions of PEKK across thermodynamic state space that will be used to inform the CG model. UA models represent all atoms in a molecule explicitly as spherical simulation elements, except for non-alcohol hydrogens, whose representations of mass and charge are “united” into the heavy elements to which they are bonded.⁴⁵ Non-bonded interactions are modeled with 12-6 Lennard-Jones potentials⁴⁶ truncated at $\sigma = 2.5$. We employ a General Amber ForceField (GAFF)⁴⁷ parameterization of the bond, angle, dihedral, and non-bonded interactions. The details of these parameterizations are available at <https://github.com/rsdefever/GAFF-foyer/tree/master/gafffoyer/xml>, which is the specific force field file imported by the present simulation workflows (<https://github.com/chrisjonesBSU/pekk-cg-model>).

Coarse-Grained PEKK

We represent each repeat unit of PEKK with three spherical simulation elements. Each element represents a phenyl ring plus its connecting group (“E” for ether, “K” for ketone, Figure 2). The resulting chain topology is a linear sequence of repeating E-K-K elements. The resulting forcefield is relatively simple, requiring parameterization of only two bond constraints, two angles, two dihedrals, and three pair-wise nonbonded interactions (Table 1).

Using this CG representation, the atomistic details of the para and meta ketone moieties are abstracted away (Figure 2), which raises the question of how to best capture the effect of

Table 1: coarse-grained model summary

Interaction	Group
Bonds	E-K, K-K
Angles	E-K-K, K-E-K
Dihedrals	E-K-K-E, K-E-K-K
Pairs	E-E, K-K, E-K

T/I ratio on PEKK polymer properties in the CG model. Keeping track of separate para- and meta- ketone simulation elements is one possible approach, but which would complicate the otherwise simple forcefield. The nonbonded interactions of these chemically identical coarse simulation elements should be similar, which raises questions about how to constrain training with MSIBI: Do we enforce identical pairwise interactions between these simulation elements, or do we allow MSIBI to find unique potentials while introducing challenges with how we interpret them? That is, because the differences in the para- and meta-linkages manifest as differences in bonded constraints between coarse simulation elements, we aim to only increase model complexity when it addresses relevant physics. To help answer these model design questions, we measure which specific components of the coarse-grained model depend on the T/I ratio, and create a coarse-graining strategy that accurately accounts for these effects only where necessary. The current body of work around CG models of Poly(ether-ketone-ketone) is relatively small. To the best of the author’s knowledge, the only other reported CG model of PEKK is presented by Chattaraj and Basu which uses a mapping scheme slightly different from this work, and doesn’t attempt to model the T/I ratio in the CG forcefield.⁴⁸

Methods

We apply one high-level method (Multi-state iterative Boltzmann inversion (MSIBI)³³), through which we implement MD simulations of UA PEKK, MD simulations of CG PEKK, and structural analysis. The resultant CG model is further validated through methods for

calculating T_g and stress relaxation times.

Molecular Dynamics Simulations

Molecular dynamics simulations of both UA and CG representations are carried out using the `Hoomd-Blue`⁴⁹ simulation engine and `signac`⁵⁰ data space management framework. Simulations are performed on the Fry high performance computing cluster at Boise State using NVIDIA P100 and V100 GPUs. All the simulations reported here, both UA and CG, are performed in the NVT ensemble (constant number of particles N , constant volume V , and constant temperature T), using the MTK velocity-verlet implementation of Nosé-Hoover chains^{51,52} with a step size of $dt = 0.0003$. We generate initial topologies using the `mBuild` python package.⁵³ We parameterize UA systems using the `foyer` python package⁵⁴ and the General Amber Forcefield (GAFF)⁴⁷ and subsequently unite hydrogen atoms into their bonded neighbors, summing their masses and partial charges into these simulation elements. No other modifications to forcefield parameters are performed. Partial charges are generated using `antechamber` with the AM1-BCC charge model,⁵⁵ and integrated using particle-particle particle-mesh (PPPM) Ewald summation.⁵⁶ Simulations are performed until equilibration as measured by autocorrelation analysis of the potential energy time series. Scripts and details of models and methods are available at <https://github.com/chrisjonesBSU/pekk-cg-model>.

Learning Coarse-Grained Potentials with MSIBI

Matching Target Distributions: Coarse-grained simulations are performed iteratively at the same thermodynamic state points as UA simulations, and the resulting structural distributions compared against the target distribution. After each iteration, the CG potentials are updated according to

$$V_{i+1}(x) = V_i(x) - \frac{1}{N} \sum_s \alpha_s k_B T_s \ln \left[\frac{P_s^i(x)}{P_s^*(x)} \right], \quad (1)$$

where V_i is the CG potential at iteration i , N is the number of state points used, α_s is a state point specific weighting factor, k_B is the Boltzmann constant, T_s is the state point temperature, and $P_s(x)$ is the structural distribution corresponding to the potential $V(x)$. $P_s^*(x)$ denotes the target distribution. In this case, the parameter α_s serves two purposes. First, it acts as a damping factor, limiting the magnitude of the potential updates at each iteration. Second, it is a state-point weighting factor where each state can be assigned a separate value of α_s which controls how much that state point influences the final potential. Iterations are run until $P_s(x)$ approaches $P_s^*(x)$ at which point $V(x)$ converges to its final form. In this work, the angle potentials are derived using a single state with $\alpha = 0.7$ over 15 IBI iterations. The inter-molecular pair potentials are obtained with all four states weighted equally, using $\alpha = 1.0$ over 20 iterations. We follow a sequential forcefield process, optimizing one forcefield component first, which is fixed during optimization of the next component. Structure-matching methods such as IBI and MSIBI typically optimize one interaction type at a time in the order of their relative strength, which follows as:^{57,58}

$$V_{stretching} \rightarrow V_{bending} \rightarrow V_{pair} \rightarrow V_{dihedral}$$

Measuring Model Success

Quantitative measurement of the match between target and coarse-grained bond, angle, dihedral and pair-wise distributions is reported using f_{fit} which is calculated by

$$f_{fit} = 1 - \frac{\sum_{x_{start}}^{x_{cut}} (|P^i(x) - P^*(x)|)}{\sum_{x_{start}}^{x_{cut}} (|P^i(x)| + |P^*(x)|)} \quad (2)$$

where $P(x)$ is the distribution resulting from the coarse-grained model and $P^*(x)$ is the target distribution.³³ In the case of a perfect match, the numerator goes to zero, and $f_{fit} = 1.0$. To quantify CG validation of chain statistics, we compare average squared radius of gyration

$\langle\langle R_g^2 \rangle\rangle$, squared end-to-end distance ($\langle\langle R_e^2 \rangle\rangle$) and persistence length ($\langle\langle L_p \rangle\rangle$) between CG and UA models. For each T/I ratio of 100/0, 80/20, 70/30, 60/40, single chain simulations of both the coarse-grained model and target model are run for 20 repeat units over a temperature range of 4.0 to 6.0 kT with increments of 0.5 kT . The persistence length measurements are performed using the MDAnalysis package.^{59,60}

Validation

The CG model of PEKK is validated against the equilibrium structural distributions of UA PEKK as described in section above, the degree to which T_g is independent of T/I ratio, and the degree to which stress relaxation times depends on T/I ratio.

In order to determine T_g of the coarse-grained model, diffusion coefficients $\mathcal{D} = \frac{dMSD}{6dt}$ are obtained directly from the trajectory's mean-square displacement (MSD). For each T/I ratio, coarse-grained simulations of 50 20-mers are run over a temperature range of 0.2 kT to 4.0 kT at increments of 0.2 kT and their MSD measured using the freud analysis package.⁶¹ For each T/I ratio, \mathcal{D} is plotted against kT and T_g is identified as the temperature where \mathcal{D} begins to diverge from $\mathcal{D} = 0$ which is indicative of the onset of polymer chain mobility. We measure the T_g in the present work with the above diffusivity criterion instead of specific-volume-based methods^{62–66} because of the relatively low equilibrium specific volume precision observed in NPT CG simulations.⁶⁷ The method is further justified by Henry *et al.*, who demonstrate that determining T_g from diffusion coefficients in CG models works and agrees with experimental measurements in thermoset polymers.⁶⁸

To validate the CG model's representation of how the T/I ratio effects T_m we simulate polymer stress relaxation and compare against experimental stress relaxation rheology. This indirect comparison is chosen due to the difficulties in measuring T_m ¹³ due to the finite size effects of the solid-liquid interface on melting. Practically, because T_m , crystallization kinetics, and relaxation times all depend on the same underlying mechanism of chain stiffness determining cooperative movement length scales,^{69–71} we focus here on relaxation dynamics

to infer the degree to which a coarse model can capture the T/I ratio effect on all three of these properties.

Rheological stress relaxation experiments were performed on an ARES G2 parallel plate rheometer (TA Instruments, New Castle, DE) with a forced air convection oven and five thermocouples to monitor the sample temperature. PEKK copolymers purchased from Arkema with T/I ratios of 60/40, 70/30, and 80/20 (Mw of 65k, MWD of 2.5, pellets. Kepstan[®] 6002, 7002, and 8002, respectively) are characterized. Stainless steel plates with a diameter of 8 mm separated by a 1.0 mm are used. Samples were loaded at 360 °C to avoid thermo-oxidative degradation. All experiments had a 1 mm gap and samples were pre-sheared to allow for homogeneity, good contact with the plates, and to remove potential air bubbles. The samples were then heated to 380°C for 3 minutes to erase any order remaining in the melt, and then cooled to 360°C. An instantaneous strain of 200.0% was applied to the samples and stress was monitored over time, collecting data at 5000 points per second to observe the rapid relaxation. The time at which 200.0% strain was reached was taken to be $t = 0$. The degree to which the stress relaxed was measured and normalized by the initial stress value at $t = 0$.

To simulate these experiments we model a PEKK volume above its T_m , apply an external strain which results in stress induced non-equilibrium chain elongation and alignment. Once the external strain is removed, the stress decay is measured as the chains relax back towards equilibrium. To qualitatively model this condition and show relaxation time trends in the coarse-grained model, for each T/I ratio we initialize systems of 200 20-mers at a density of $1/38 \frac{g}{cm^3}$ where the chains begin in a non-equilibrium elongated and aligned state. Each system is held at the same temperature of $2.0kT$ while the chains relax from the initial non-equilibrium state to an equilibrium state. To show chain relaxation time trends, we measure the decay of an order parameter rather than measuring stress directly. We use the nematic order parameter as a measurement of chain backbone linearity and the decay of the nematic order over time as a qualitative analog to stress relaxation decay from experimental results.

Nematic order, also referred to as the S_2 order parameter, is a description of orientational ordering, and is often used as a measurement of polymer chain alignment^{72,73} and experimental work has shown a relationship between nematic order and equilibraiton relaxation times.^{70,71} The `freud` python library is used to calculate the nematic order parameter.⁶¹ In summary, the success of the coarse-grained model across the T/I ratio range will be measured structurally and dynamically. First, we determine if the bonded and non-bonded structural distributions are accurately re-created. Second, we ensure that key polymer chain statistical metrics are sufficiently reproduced in the coarse-grained model; this includes the single-chain radius of gyration (R_g), end-to-end distance (R_{EE}) and persistence length (P_l). Third, we test the hypothesis that the coarse model can capture the T/I ratio effect by varying only one aspect of the overall force-field.

Results and Discussion

We report on the structural distributions observed in UA simulations and discuss the role of T/I ratio.

United Atom simulations

Single chain UA simulations are run to obtain the target bond length, angle, and dihedral distributions used for generating the CG bonded potentials. Chain lengths of 20 repeat units are run at a low density of $0.0003 \frac{g}{cm^3}$ (i.e. vacuum) at a temperature of $415^\circ C$. The single chain simulations ran for 7.3 ns with a time step of 0.145 fs . In order to observe the effect the T/I ratio has on the bonded interactions, simulations are performed for each T/I ratio of 100/0, 80/20, 70/30 and 60/40. The sequence of T and I monomers are assigned randomly down the length of the polymer chain, weighted by the target T/I ratio. In order to ensure effective sampling, five different random sequences are generated for each T/I ratio with single-chain simulations run separately for each sequence. We measure the bond length, an-

gle and dihedral distributions for each T/I ratio by averaging over the replicate single chain trajectories.

Bulk systems of 50 PEKK oligomers consisting of six repeat units using a T/I ratio of 100/0 are run to obtain the target radial distribution functions needed for generating the coarse-grained pair potentials. Only a single T/I ratio is used, as we expect any significant differences in pair-wise distributions as a function of T/I ratio to ultimately be the result of chain structures arising from intra-chain interactions. In other words, the presence of meta linkages does not create differences in the chemical makeup or mapping of our coarse-grained beads in a way such that their underlying pair interactions are effectively different. Polymers below typical molecular weight values for PEKK are used in order to increase computational efficiency in reaching equilibrated target trajectories. Previous work shows that coarse-grained pair potentials derived from oligomers are transferable to systems of larger molecular weights.⁷⁴ The state points used are described in Table 2. State point **A** is a unique case where the system consists of two chains of 16 repeat units each in a vacuum. State points **B**, **C** and **D** include two states with a temperature half-way between T_g and T_m at reported values for both amorphous and crystalline densities, and a state above melting at an amorphous density.⁷⁵

Table 2: United atom simulations are performed at four thermodynamic states spanning two temperatures and three densities.

State	Temperature C°	Density $\frac{g}{cm^3}$
A	414	0.0003
B	255	1.27
C	255	1.35
D	414	1.27

The bond, angle and dihedral distributions as a function of the T/I ratio obtained from the target single-chain trajectories are shown in Figure 3. The bond length and dihedral distributions appear relatively non-sensitive to the T/I ratio. The **E-K** bond distributions are

nearly identical over the entire T/I ratio range, and we do not consider the slight variance in the **K-K** bond length distribution width large enough to significantly affect the bulk structure or properties of the coarse-grained model.⁷⁶ Additionally, the **K-E-K** angle distribution shows no notable dependence on the T/I ratio. Significant differences arise in the **E-K-K** angle distribution which clearly exhibits the most sensitivity to the T/I ratio with an emergence of a second peak near 1.3 radians once the T/I ratio drops below 1.0. The intensity of this second, smaller angle peak, grows as the T/I ratio decreases, while the peak at 2.2 radians decreases.

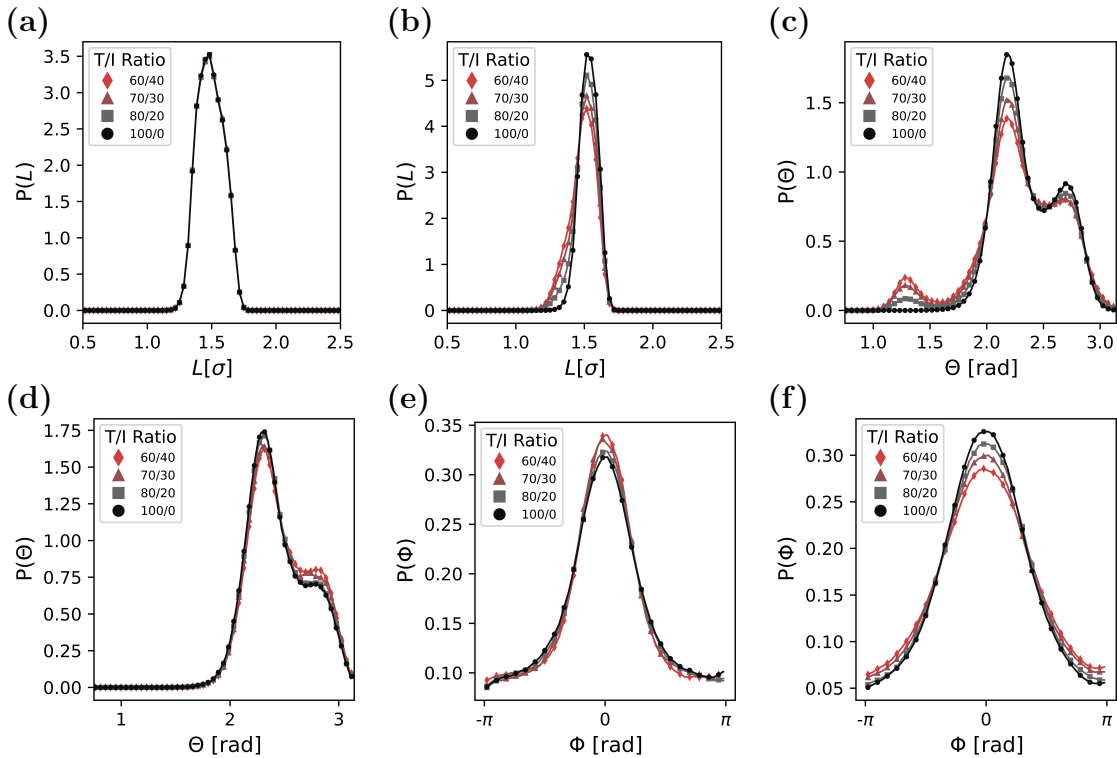


Figure 3: Intra-chain distributions from united atom, single-chain simulations at a reduced temperature of $6.5 kT$. (a) E-K bonds, (b) K-K bonds, (c) E-K-K angles, (d) K-E-K angles, (e) E-K-K-E dihedrals, and (f) K-E-K-K dihedrals. The E-K-K angle distribution is the only one to significantly change shape with T/I ratio.

Coarse-grained Model

Coarse-grained Potentials

Figure 4 highlights the angle and pair potentials resulting from IBI and MSIBI respectively. The **E-K-K** angle potential shows an emergence of a second, meta-stable energy well at smaller angles. Additionally, the energy barrier between the large-angle and small-angle wells appears to slightly decrease with decreasing T/I ratios. For the **K-E-K** angle, we only derive a single potential that is used across all T/I ratios modelled in this work. Potentials that result from IBI and MSIBI don't necessarily follow any functional form, and can often have nonphysical shapes such as multiple wells and peaks. Here, we find sensible potentials that are consistent with a soft-core Lennard Jones-like pair potential.

The **E-E** and **E-K** pair potentials exhibit similar shapes with the **E-E** beads having a slightly smaller effective radius and deeper energy well.

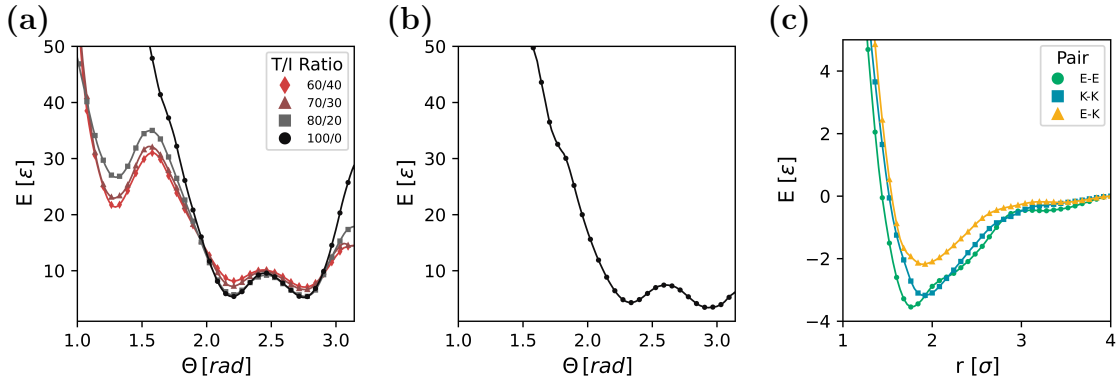


Figure 4: Potentials obtained from MSIBI for the CG PEKK model. The EKK angle potential (a) shows a dependence on the T/I ratio of the PEKK polymers while the KEK angle potential (b) does not. The non-bonded pair potentials (c) are shown all three bead type interactions.

Coarse-grained Model Performance

Figure 5 illustrates the pair-wise RDF comparison between the coarse-grained and united-atom models for each pair across all four states. Good agreement between the distributions is observed at all four state points. The detailed f_{fit} score obtained using Equation 2 are summarized in Table S3 of the supplementary information.

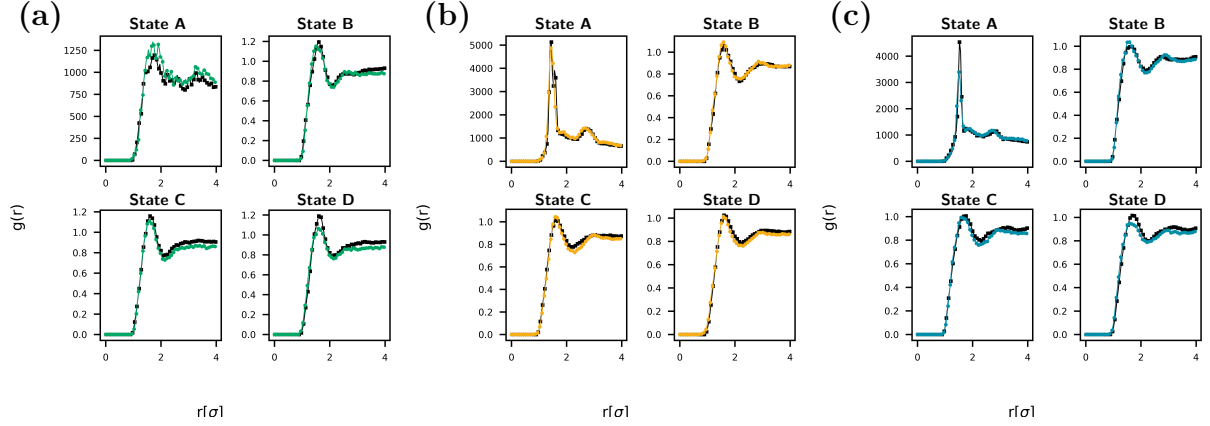


Figure 5: Comparison between RDFs obtained from the U.A. model target (black lines) and the C.G. model (colored lines). RDFs from each state are shown for pairs E-E (a), E-K (b) and K-K (c).

Figure 6 shows the performance in matching the single-chain bond-angle distributions over the T/I ratio range. The CG model is able to accurately reproduce the emergence of smaller angle peaks with decreasing large angle peaks for the **E-K-K** angle while achieving f_{fit} values of 0.98 or larger at each T/I ratio. The **K-E-K** distributions across the T/I ratio range are also accurately recreated. The detailed f_{fit} values are summarized in Table SX.

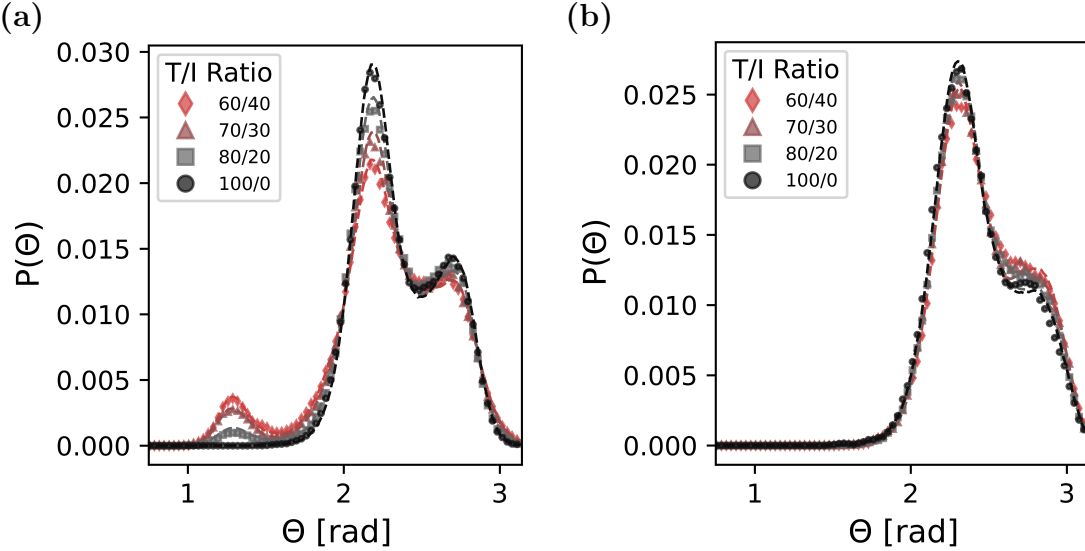


Figure 6: Comparison of target E-K-K (a) and K-E-K (b) angle distributions (dashed lines) and CG model angle distributions (symbols). We see good agreement for both across all T/I ratios studied.

Transferability

Chain Structure

Figure 7 reports the measured results for persistence-length (l_P), squared end-to-end distance (R_e^2) and squared radius of gyration (R_g^2) for a single T/I ratio of 0.80 across a reduced temperature span of $4 kT$ to $6 kT$. Figure 8 shows the same measurements at a constant reduced temperature of $5.0 kT$ over the T/I ratio range studied. In both cases, excellent agreement between the U.A. and C.G. models is observed for all three values measured. Interestingly, and perhaps counter-intuitively, is the fact that no clear trends are observed in the chain statistic measurements as the T/I ratio is changed in either model. Unfortunately, experimental data for these proprieties are not easily found, so we are unable to identify if the lack of a trend is to be expected, or an indication that the model is missing some of the underlying physics that governs PEKK polymer conformations.

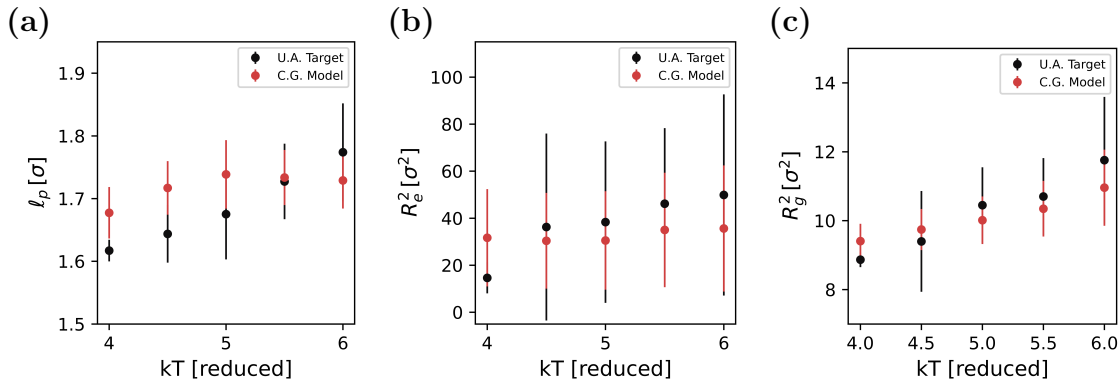


Figure 7: Persistance length (a), squared end-to-end distance (b) and squared radius of gyration (c) comparisons are shown over a temperature range with a T/I ratio of 0.80.

Capturing Effect of the T/I Ratio

Figure 9 shows the self-diffusion coefficient over a range of temperatures of the CG model for each T/I ratio. Where the D_{self} transitions from zero to non-zero is indicative of the onset of T_g .^{68,77} We can see that the transition point shows no significant changes based on the T/I ratio, which is consistent with the expectations of T_g in PEKK being insensitive to

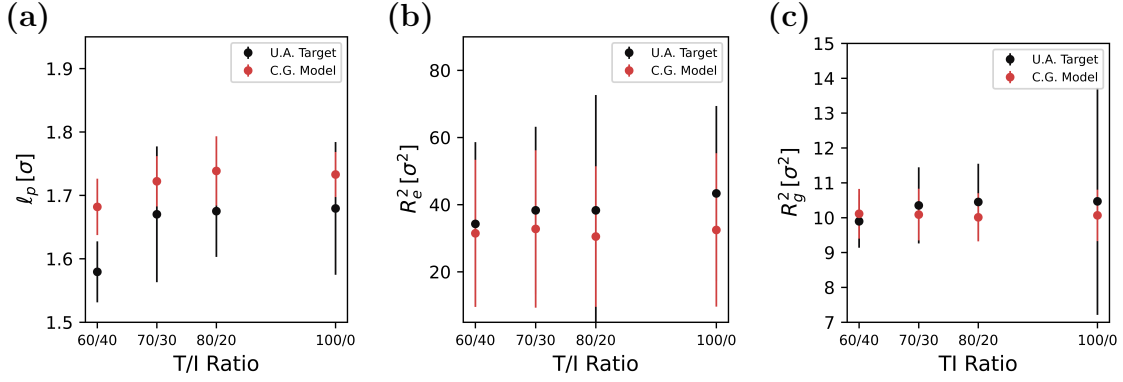


Figure 8: Persistance length (a), squared end-to-end distance (b) and squared radius of gyration (c) comparisons are shown over the T/I ratio range studied at a constant reduced temperature of $5.0 kT$.

T/I ratio.

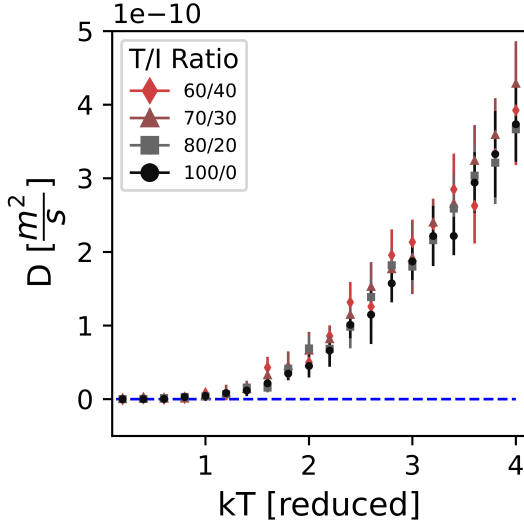


Figure 9: Self-diffusion coefficients measured across several temperatures for each T/I ratio.

In Figure 10 we show a comparison between chain relaxation times as a function of T/I ratio between the CG computational model, and experimental results obtained from rheological stress relaxation. While these two experiments are measuring different properties, they both are ultimately measuring the same relaxation process from non-equilibrium states to relaxed states. Both measurements, S2 order parameter decay in the computational model, and stress decay in the experiments, clearly show a dependence on the T/I ratio where polymer melts with larger T/I ratios relax more slowly than those with lower T/I ratios. While the

computational model cannot access the same time scales as experiments, this consistency between experiment and computational models is encouraging. By encoding the T/I ratio in the **E-K-K** angle potential (Figure 4 (a))

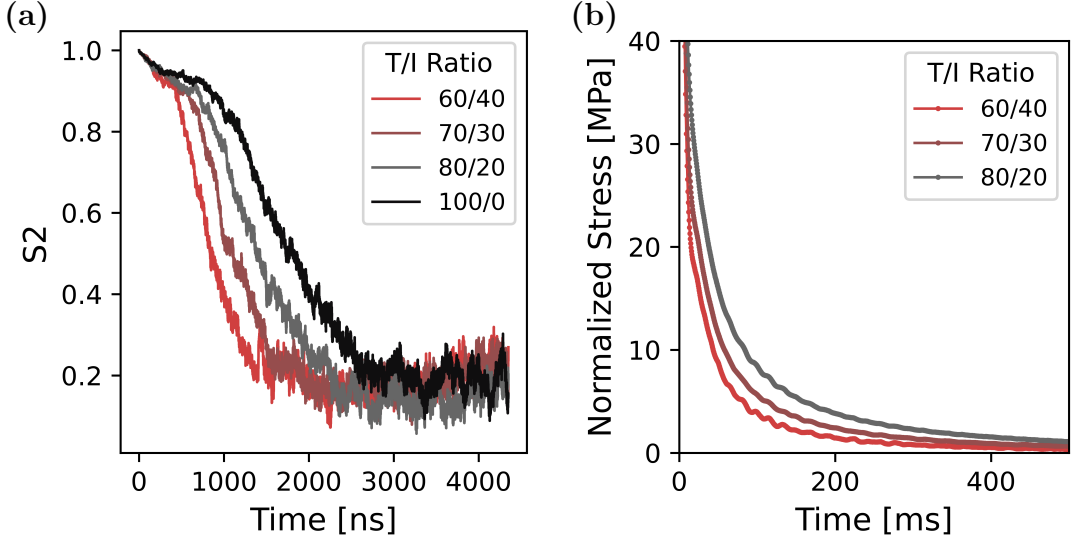


Figure 10: Qualitative comparison of chain relaxation times as a function of T/I ratio with (a) Nematic order parameter decay of the C.G. model and (b) normalized stress decay from experimental results.

Computational Performance

The TPS values are obtained using NVIDIA Tesla-P100 GPUs with 12GB of VRAM, and the comparison between U.A. and C.G. models, and how each scales with system size, are shown in Figure 11. TPS improvement ranges from a factor of two at small system sizes, to a factor of nearly 15 at system sizes of 30,000 monomers, where the C.G. model has a TPS of 851 while the U.A. model is only 54 TPS.

The difference between angle distributions observed during fine-grain simulations was captured by the MSIBI method as a difference in the angle potentials for the CG system. The most obvious difference is the presence of a small peak centered around 1.2 radians in the E-K-K angle distribution, which is absent in the K-E-K distribution. Along with the RDFs from the all atom simulations, this indicates that the T/I ratio directly affects the final equilibrium configuration of the polymer, and its dynamics. We can see that the coarse-

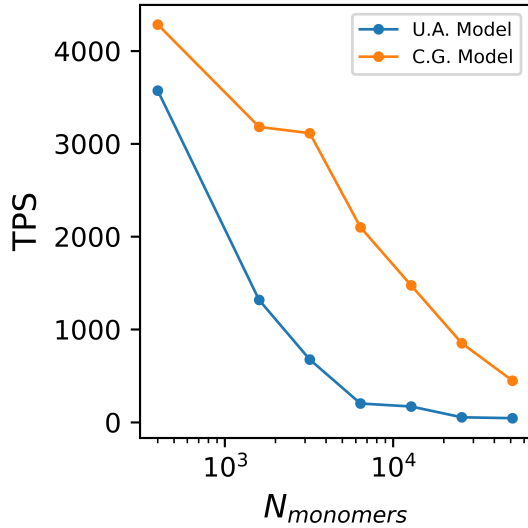


Figure 11: Timesteps per second comparison between the united atom (UA) and coarse-grained (CG) models run on NVIDIA Tesla-P100 GPUs.

grained potentials reflect and preserve these differences while reducing degrees of freedom and speeding up simulation by and order of 10 to 15.

Conclusions

The CG model of PEKK demonstrated here is able to successfully recreate bulk morphology, intra-chain distributions, and the key polymer structural parameters of radius of gyration, end-to-end distance, and persistence length obtained from target UA simulations, while achieving substantial computational efficiency improvements compared to the UA model. The CG model of PEKK shows similar values for T_g across all T/I ratios of 100/0, 80/20, 70/30 and 60/40, and also qualitatively captures experimental stress relaxation behavior as a function of T/I ratio. We demonstrate that the T/I ratio effect observed experimentally in PEKK, and crucial for multiscale computational modeling efforts of PEKK, can be encoded in a single forcefield component, which in the case of the mapping scheme used in this work, is the **E-K-K** angle potential (Figure 4 (a)). This approach results in a general CG model of PEKK that is transferrable to various T/I ratios where the CG forcefield is given by

$$U_{CG} = U_{EK,KK}(\ell) + U_{KEK}(\theta) + U_{KEK} \left(\theta, \frac{T}{I} \right) + U_{EKKE,KEKK}(\phi) + U_{EE,KK,EK}(r_i, r_j) \quad (3)$$

where changing only the tabulated potential for $U_{EKK}(\theta, \frac{T}{I})$ determines the T/I ratio being modelled. Here, we derive $U_{EKK}(\theta, \frac{T}{I})$ for T/I ratios of 100/0, 80/20, 70/30 and 60/40, which represent the most commonly used, and commercially available PEKK polymers; however, the approach we demonstrate provides the ability to model any T/I ratio of PEKK. This model is easily extensible, where obtaining new potentials for $U_{EKK}(\theta, \frac{T}{I})$ would only require running a single chain UA simulation followed by a short IBI optimization of only one interaction—both of which are computationally inexpensive tasks. Furthermore, perhaps this strategy is generally applicable to capturing structural isomer affects in CG models of other polymers containing phenylene backbones, such as poly(phenylensulfide), poly(phenylenediamine), and other polymers in the polyaryletherketone family of thermoplastics.

These models demonstrate significant computational performance improvements, enabling the investigation of PEKK entanglement dynamics at far more practical time scales.

References

- (1) Yao, S.-S.; Jin, F.-L.; Rhee, K. Y.; Hui, D.; Park, S.-J. Recent advances in carbon-fiber-reinforced thermoplastic composites: A review. *Composites Part B: Engineering* **2018**, *142*, 241–250.
- (2) Avenet, J.; Cender, T. A.; Corre, S. L.; Bailleul, J.-L.; Levy, A. Adhesion of High Temperature Thermoplastic Composites. *Procedia Manufacturing* **2020**, *47*, 925–932.
- (3) Doll, G. Thermoplastic composites technologies for future aircraft structures. Vehicles of Tomorrow 2019. Wiesbaden, 2021; pp 129–138.

- (4) Barroeta Robles, J.; Dubé, M.; Hubert, P.; Yousefpour, A. Repair of thermoplastic composites: an overview. *Advanced Manufacturing: Polymer & Composites Science* **2022**, *8*, 68–96.
- (5) Ghanbari, L. N.; Crater, E. R.; Enos, N. R.; McNair, O. D.; Moore, R. B.; Wiggins, J. S. Polyphenylene sulfide for high-rate composite manufacturing: Impacts of processing parameters on chain architecture, rheology, and crystallinity. *Polymer Degradation and Stability* **2023**, *218*, 110580, tex.ids= Ghanbari:2023:PolymerDegradationandStability, Ghanbari:2023:PolymerDegradationandStabilitya.
- (6) Barile, M.; Lecce, L.; Iannone, M.; Pappadà, S.; Roberti, P. In *Revolutionizing Aircraft Materials and Processes*; Pantelakis, S., Tserpes, K., Eds.; Springer International Publishing: Cham, 2020; pp 87–114, tex.ids= Barile:2020:RevolutionizingAircraftMaterialsandProcessesa.
- (7) Gardiner, G. Welding is not bonding. 2024; <https://www.compositesworld.com/articles/welding-is-not-bonding>.
- (8) Ge, T.; Pierce, F.; Perahia, D.; Grest, G. S.; Robbins, M. O. Molecular dynamics simulations of polymer welding: Strength from interfacial entanglements. *Physical Review Letters* **2013**, *110*, 1–5, tex.ids= Ge:2013:Phys.Rev.Lett., Ge:2013:Phys.Rev.Lett.a.
- (9) Alfonso, G. C.; Russell, T. P. Kinetics of crystallization in semicrystalline/amorphous polymer mixtures. *Macromolecules* **1986**, *19*, 1143–1152.
- (10) Basire, C.; Ivanov, D. A. Evolution of the Lamellar Structure during Crystallization of a Semicrystalline-Amorphous Polymer Blend: Time-Resolved Hot-Stage SPM Study. *Physical Review Letters* **2000**, *85*, 5587–5590.
- (11) Choupin, T.; Fayolle, B.; Régnier, G.; Paris, C.; Cinquin, J.; Brûlé, B. Isothermal crystallization kinetic modeling of poly(etherketoneketone) (PEKK) copolymer. *Polymer* **2017**, *111*, 73–82, tex.ids= choupinIsothermalCrystallizationKinetic2017a.

- (12) Pérez-Martín, H.; Mackenzie, P.; Baidak, A.; Ó Brádaigh, C. M.; Ray, D. Crystallinity studies of PEKK and carbon fibre/PEKK composites: A review. *Composites Part B: Engineering* **2021**, *223*, 109127.
- (13) Wan, S.; Sinclair, R. C.; Coveney, P. V. Uncertainty quantification in classical molecular dynamics. *Philosophical Transactions of the Royal Society A: Mathematical, Physical and Engineering Sciences* **2021**, *379*, rsta.2020.0082, 20200082.
- (14) Joshi, S. Y.; Deshmukh, S. A. A review of advancements in coarse-grained molecular dynamics simulations. *Molecular Simulation* **2021**, *47*, 786–803.
- (15) Ge, T.; Grest, G. S.; Robbins, M. O. Structure and Strength at Immiscible Polymer Interfaces. *ACS Macro Letters* **2013**, *2*, 882–886.
- (16) Ge, T.; Grest, G. S.; Robbins, M. O. Tensile Fracture of Welded Polymer Interfaces: Miscibility, Entanglements, and Crazing. *Macromolecules* **2014**, *47*, 6982–6989.
- (17) Thomas, S.; Alberts, M.; Henry, M. M.; Estridge, C. E.; Jankowski, E. Routine million-particle simulations of epoxy curing with dissipative particle dynamics. *Journal of Theoretical and Computational Chemistry* **2018**, *17*, 1840005.
- (18) Thomas, S. New Methods for Understanding and Controlling the Self-Assembly of Reacting Systems Using Coarse-Grained Molecular Dynamics. Ph.D. thesis, Boise State University, 2018.
- (19) Edwards, S. F. Statistical mechanics with topological constraints: I. *Proceedings of the Physical Society* **1967**, *91*, 513–519.
- (20) De Gennes, P. G. Reptation of a Polymer Chain in the Presence of Fixed Obstacles. *The Journal of Chemical Physics* **1971**, *55*, 572–579.
- (21) Gartner, T. E.; Jayaraman, A. Modeling and Simulations of Polymers: A Roadmap. *Macromolecules* **2019**, *52*, 755–786.

- (22) Dhamankar, S.; Webb, M. A. Chemically specific coarse-graining of polymers: Methods and prospects. *Journal of Polymer Science* **2021**, *59*, 2613–2643.
- (23) Izvekov, S.; Voth, G. A. Multiscale coarse graining of liquid-state systems. *The Journal of Chemical Physics* **2005**, *123*, 134105.
- (24) Hynninen, A.-P.; Matthews, J. F.; Beckham, G. T.; Crowley, M. F.; Nimlos, M. R. Coarse-Grain Model for Glucose, Cellobiose, and Cellotetraose in Water. *Journal of Chemical Theory and Computation* **2011**, *7*, 2137–2150.
- (25) Shell, M. S. The relative entropy is fundamental to multiscale and inverse thermodynamic problems. *The Journal of Chemical Physics* **2008**, *129*, 144108.
- (26) Chaimovich, A.; Shell, M. S. Coarse-graining errors and numerical optimization using a relative entropy framework. *The Journal of Chemical Physics* **2011**, *134*, 094112.
- (27) Reith, D.; Pütz, M.; Müller-Plathe, F. Deriving effective mesoscale potentials from atomistic simulations: Mesoscale Potentials from Atomistic Simulations. *Journal of Computational Chemistry* **2003**, *24*, 1624–1636.
- (28) Tscho, W.; Kremer, K.; Batoulis, J.; Bu, T.; Hahn, O.; Ju, F.; Alto, P. Simulation of polymer melts. I. Coarse-graining procedure for polycarbonates. *Acta Polymerica* **1998**, *61*–74, ISBN: 4961313793.
- (29) Peters, B. L.; Salerno, K. M.; Agrawal, A.; Perahia, D.; Grest, G. S. Coarse-Grained Modeling of Polyethylene Melts: Effect on Dynamics. *Journal of Chemical Theory and Computation* **2017**, *13*, 2890–2896.
- (30) Milano, G.; Müller-Plathe, F. Mapping Atomistic Simulations to Mesoscopic Models: A Systematic Coarse-Graining Procedure for Vinyl Polymer Chains. *The Journal of Physical Chemistry B* **2005**, *109*, 18609–18619, tex.ids= milanoMappingAtomisticSimulations2005.

- (31) León, S.; Vegt, N. V. D.; Site, L. D.; Kremer, K. Bisphenol a polycarbonate: Entanglement analysis from coarse-grained MD simulations. *Macromolecules* **2005**, *38*, 8078–8092.
- (32) Zhang, X.-Z.; Lu, Z.-Y.; Qian, H.-J. Temperature Transferable and Thermodynamically Consistent Coarse-Grained Model for Binary Polymer Systems. *Macromolecules* **2023**, *56*, 3739–3753.
- (33) Moore, T. C.; Iacovella, C. R.; McCabe, C. Derivation of coarse-grained potentials via multistate iterative Boltzmann inversion. *The Journal of Chemical Physics* **2014**, *140*, 224104, tex.ids= Moore:2014:J.Chem.Phys.
- (34) Moore, T. C.; Iacovella, C. R.; McCabe, C. Development of a Coarse-Grained Water Forcefield via Multistate Iterative Boltzmann Inversion. **2016**, 37–52, tex.ids= moore-DevelopmentCoarsegrainedWater2015 ISBN: 9789811011283.
- (35) Moore, T. C.; Iacovella, C. R.; Hartkamp, R.; Bunge, A. L.; McCabe, C. A Coarse-Grained Model of Stratum Corneum Lipids: Free Fatty Acids and Ceramide NS. *Journal of Physical Chemistry B* **2016**, *120*, 9944–9958.
- (36) Moore, T. C.; Iacovella, C. R.; Leonhard, A. C.; Bunge, A. L.; McCabe, C. Molecular dynamics simulations of stratum corneum lipid mixtures: A multiscale perspective. *Biochemical and Biophysical Research Communications* **2018**, *498*, 313–318, Publisher: Elsevier Ltd.
- (37) Shamatprasad, P.; Moore, T. C.; Xia, D.; Iacovella, C. R.; Bunge, A. L.; McCabe, C. Multiscale Simulation of Ternary Stratum Corneum Lipid Mixtures: Effects of Cholesterol Composition. *Langmuir* **2022**, *38*, 7496–7511.
- (38) Quiroga Cortés, L.; Caussé, N.; Dantras, E.; Lonjon, A.; Lacabanne, C. Morphology and dynamical mechanical properties of poly ether ketone ketone (PEKK) with meta phenyl links. *Journal of Applied Polymer Science* **2016**, *133*, n/a–n/a.

- (39) Choupin, T.; Fayolle, B.; Paris, C.; Cinquin, J.; Innovations, A. G.; Departement, C. M.; Rilsan, R. Mechanical Performances of Pekk Composite. **2017**, 20–25.
- (40) Gardner, K. H.; Hsiao, B. S.; Matheson, R. R.; Wood, B. A. Structure, crystallization and morphology of poly (aryl ether ketone ketone). *Polymer* **1992**, *33*, 2483–2495.
- (41) Li, C.; Strachan, A. Prediction of PEKK properties related to crystallization by molecular dynamics simulations with a united-atom model. *Polymer* **2019**, *174*, 25–32, tex.ids= liPredictionPEKKProperties2019, liPredictionPEKKProperties2019a publisher: Elsevier.
- (42) White, K. L.; Jin, L.; Ferrer, N.; Wong, M.; Bremner, T.; Sue, H. Rheological and thermal behaviors of commercial poly(aryletherketone)s. *Polymer Engineering & Science* **2013**, *53*, 651–661.
- (43) Bonmatin, M.; Chabert, F.; Bernhart, G.; Djilali, T. Rheological and crystallization behaviors of low processing temperature poly(aryl ether ketone). *Journal of Applied Polymer Science* **2021**, *138*, 51402.
- (44) Croshaw, C.; Hamernik, L.; Ghanbari, L.; Browning, A.; Wiggins, J. Melt-state degradation mechanism of poly (ether ketone ketone): the role of branching on crystallization and rheological behavior. *Polymer Degradation and Stability* **2022**, *200*, 109968.
- (45) Jorgensen, W. L.; Tirado-Rives, J. The OPLS [optimized potentials for liquid simulations] potential functions for proteins, energy minimizations for crystals of cyclic peptides and crambin. *Journal of the American Chemical Society* **1988**, *110*, 1657–1666.
- (46) Lennard-Jones, J. The electronic structure of some diatomic molecules. *Transactions of the Faraday Society* **1929**, *25*, 668–686.

- (47) Wang, J.; Wolf, R. M.; Caldwell, J. W.; Kollman, P. A.; Case, D. A. Development and testing of a general amber force field. *Journal of Computational Chemistry* **2004**, *25*, 1157–1174.
- (48) Chattaraj, S.; Basu, S. Coarse-graining strategies for predicting properties of closely related polymer architectures: A case study of PEEK and PEKK. *Journal of Materials Research* **2021**, ISBN: 0123456789 Publisher: Springer International Publishing.
- (49) Anderson, J. A.; Glaser, J.; Glotzer, S. C. HOOMD-blue: A Python package for high-performance molecular dynamics and hard particle Monte Carlo simulations. *Computational Materials Science* **2020**, *173*, 109363, tex.ids= Anderson:2020:ComputationalMaterialsScience, andersonHOOMDbluePythonPackage2020.
- (50) Adorf, C. S.; Dodd, P. M.; Ramasubramani, V.; Glotzer, S. C. Simple data and workflow management with the signac framework. *Computational Materials Science* **2018**, *146*, 220–229, tex.ids= Adorf:2018:ComputationalMaterialsScience.
- (51) Martyna, G. J.; Tobias, D. J.; Klein, M. L. Constant pressure molecular dynamics algorithms. *The Journal of Chemical Physics* **1994**, *101*, 4177–4189.
- (52) Cao, J.; Martyna, G. J. Adiabatic path integral molecular dynamics methods. II. Algorithms. *The Journal of Chemical Physics* **1996**, *104*, 2028–2035.
- (53) Klein, C.; Sallai, J.; Jones, T. J.; Iacobella, C. R.; McCabe, C.; Cummings, P. T. In *Foundations of Molecular Modeling and Simulation*; Snurr, R. Q., Adjiman, C. S., Kofke, D. A., Eds.; Springer Singapore: Singapore, 2016; pp 79–92, tex.ids= Klein:2016:FoundationsofMolecularModelingandSimulation seriesTitle: Molecular Modeling and Simulation.
- (54) Klein, C.; Summers, A. Z.; Thompson, M. W.; Gilmer, J. B.; McCabe, C.; Cummings, P. T.; Sallai, J.; Iacobella, C. R. Formalizing atom-typing and the dissemination

- of force fields with foyer. *Computational Materials Science* **2019**, *167*, 215–227, tex.ids=Klein:2019:ComputationalMaterialsScience.
- (55) Jakalian, A.; Jack, D. B.; Bayly, C. I. Fast, efficient generation of high-quality atomic charges. AM1-BCC model: II. Parameterization and validation. *Journal of Computational Chemistry* **2002**, *23*, 1623–1641, tex.ids= Jakalian:2002:JComputChema.
- (56) LeBard, D. N.; Levine, B. G.; Mertmann, P.; Barr, S. A.; Jusufi, A.; Sanders, S.; Klein, M. L.; Panagiotopoulos, A. Z. Self-assembly of coarse-grained ionic surfactants accelerated by graphics processing units. *Soft Matter* **2012**, *8*, 2385–2397, Publisher: The Royal Society of Chemistry.
- (57) Reith, D.; Meyer, H.; Müller-Plathe, F. Mapping atomistic to coarse-grained polymer models using automatic simplex optimization to fit structural properties. *Macromolecules* **2001**, *34*, 2335–2345.
- (58) Hsu, D. D.; Xia, W.; Arturo, S. G.; Keten, S. Thermomechanically consistent and temperature transferable coarse-graining of atactic polystyrene. *Macromolecules* **2015**, *48*, 3057–3068, tex.ids= hsuThermomechanicallyConsistentTemperature2015a, hsuThermomechanicallyConsistentTemperature2015b.
- (59) Gowens, R.; Linke, M.; Barnoud, J.; Reddy, T.; Melo, M.; Seyler, S.; Domański, J.; Dotson, D.; Buchoux, S.; Kenney, I.; Beckstein, O. MDAnalysis: A Python Package for the Rapid Analysis of Molecular Dynamics Simulations. Austin, Texas, 2016; pp 98–105.
- (60) Michaud-Agrawal, N.; Denning, E. J.; Woolf, T. B.; Beckstein, O. MDAnalysis: A toolkit for the analysis of molecular dynamics simulations. *Journal of Computational Chemistry* **2011**, *32*, 2319–2327.
- (61) Ramasubramani, V.; Dice, B. D.; Harper, E. S.; Spellings, M. P.; Anderson, J. A.;

- Glotzer, S. C. freud: A software suite for high throughput analysis of particle simulation data. *Computer Physics Communications* **2020**, *254*, 107275.
- (62) Takeuchi, H.; Roe, R.-J. Molecular dynamics simulation of local chain motion in bulk amorphous polymers. II. Dynamics at glass transition. *The Journal of Chemical Physics* **1991**, *94*, 7458–7465.
- (63) Roe, R.-J. In *Atomistic Modeling of Physical Properties*; Monnerie, L., Suter, U. W., Eds.; Springer Berlin Heidelberg, 1994; Vol. 116; pp 111–144, Series Title: Advances in Polymer Science.
- (64) Dudowicz, J.; Freed, K. F.; Douglas, J. F. The Glass Transition Temperature of Polymer Melts. *The Journal of Physical Chemistry B* **2005**, *109*, 21285–21292.
- (65) Patrone, P. N.; Dienstfrey, A.; Browning, A. R.; Tucker, S.; Christensen, S. Uncertainty quantification in molecular dynamics studies of the glass transition temperature. *Polymer* **2016**, *87*, 246–259.
- (66) Mohammadi, M.; Fazli, H.; Karevan, M.; Davoodi, J. The glass transition temperature of PMMA: A molecular dynamics study and comparison of various determination methods. *European Polymer Journal* **2017**, *91*, 121–133, tex.ids= Mohammadi:2017:EuropeanPolymerJournal, mohammadiGlassTransitionTemperature2017b.
- (67) Fu, C.-C.; Kulkarni, P. M.; Scott Shell, M.; Gary Leal, L. A test of systematic coarse-graining of molecular dynamics simulations: Thermodynamic properties. *The Journal of Chemical Physics* **2012**, *137*, 164106.
- (68) Henry, M. M.; Thomas, S.; Alberts, M.; Estridge, C. E.; Farmer, B.; McNair, O.; Jankowski, E. General-Purpose Coarse-Grained Toughened Thermoset Model for 44DDS/DGEBA/PES. *Polymers* **2020**, *12*, 2547.

- (69) Bunn, C. W. The melting points of chain polymers. *Journal of Polymer Science Part B: Polymer Physics* **1996**, *34*, 799–819.
- (70) Ohzono, T.; Katoh, K.; Minamikawa, H.; Saed, M. O.; Terentjev, E. M. Internal constraints and arrested relaxation in main-chain nematic elastomers. *Nature Communications* **2021**, *12*, 787.
- (71) Hotta, A.; Terentjev, E. M. Long-time stress relaxation in polyacrylate nematic liquid crystalline elastomers. *Journal of Physics: Condensed Matter* **2001**, *13*, 11453–11464.
- (72) Sigaud, G.; Yoon, D. Y.; Griffin, A. C. Order in nematic phase of semiflexible polymers. *Macromolecules* **1983**, *16*, 875–880.
- (73) Hu, W.; Frenkel, D. In *Interphases and Mesophases in Polymer Crystallization III*; Allegra, G., Ed.; Springer-Verlag: Berlin/Heidelberg, 2005; Vol. 191; pp 1–35, Series Title: Advances in Polymer Science.
- (74) Choudhury, C. K.; Carbone, P.; Roy, S. Scalability of Coarse-Grained Potentials Generated from Iterative Boltzmann Inversion for Polymers: Case Study on Polycarbonates. *Macromolecular Theory and Simulations* **2016**, *25*, 274–286, tex.ids= choudhuryScalabilityCoarseGrainedPotentials2016a.
- (75) Tencé-Girault, S.; Quibel, J.; Cherri, A.; Roland, S.; Fayolle, B.; Bizet, S.; Iliopoulos, I. Quantitative Structural Study of Cold-Crystallized PEKK. *ACS Applied Polymer Materials* **2021**, *3*, 1795–1808.
- (76) Vettorel, T.; Meyer, H. Coarse graining of short polyethylene chains for studying polymer crystallization. *Journal of Chemical Theory and Computation* **2006**, *2*, 616–629.
- (77) Bulacu, M.; van der Giessen, E. Molecular-dynamics simulation study of the glass transition in amorphous polymers with controlled chain stiffness. *Physical Review E* **2007**, *76*, 011807, tex.ids= Bulacu:2007:Phys.Rev.E.